ATOMIC FORCE MICROSCOPY AT ULTRASONIC FREQUENCIES

W. Arnold, A. Caron, S. Hirsekorn,
M. Kopycinska-Müller, U. Rabe, and M. Reinstädtler*

I. INTRODUCTION

Atomic Force Microscopy (AFM) is a near-field technique to generate high-resolution images of surfaces. A micro-fabricated elastic beam with an integrated sharp sensor tip at its end is scanned over the sample surface. With various dynamic modes, leading to Force Modulation Microscopy [1], Ultrasonic Force Microscopy [2], Atomic Force Acoustic Microscopy (AFAM) [3–5], Microdeformation Microscopy [6], Scanning Local Acceleration Microscopy [7] or Pulsed Force Microscopy [8], images can be obtained in which the contrast depends on the elasticity of the sample surface. However, quantitative determination of Young's modulus of a sample surface with AFM is a challenge, especially when stiff materials such as hard metals or ceramics are encountered. In this presentation the basic idea of AFAM, i.e. the evaluation of the cantilever vibration spectra at ultrasonic frequencies is discussed. The AFAM technique can be used for imaging as well as to discern local elastic data quantitatively. Nanocrystalline magnetic materials [9], multidomain piezoelectric materials and silicon [10], diamond-like carbon layers [11], polymeric materials and clay crystals [12] have been examined previously. The spatial resolution of the AFAM technique is approximately 10 nm.

In an Atomic Force Acoustic Microscopy set-up [3-5] either the sample is insonified or the cantilever suspension is excited at ultrasonic frequencies. The vibration spectra of the cantilever depend on the local sample stiffness and hence

* Fraunhofer-Institute for Nondestructive Testing (IZFP), Bldg. 37, University, D-66123 Saarbrücken, Germany

on the local elasticity of the sample constituents. Acoustic images can be obtained by measuring the cantilever vibration amplitude at a frequency close to a contact resonance or by monitoring the resonance frequency [13,14]. With this technique it is possible to resolve the differences in the local tip-sample stiffness between phases and/or grains having different crystal lattice orientation. In the case of ferroelectric materials the presence of the domains influences the local elastic properties within each individual grain. Depending on the method of sample preparation, for example etching, one can make domain patterns visible on the sample surface using AFM [15]. In this case the contrast is caused by topography. A variety of AFM techniques have been applied to image or modify the domains in ferro- electric single crystals as well as in thin films [16,17]. The AFAM technique allows domain structure imaging in single crystals and in ceramics, even when domains do not appear in the topography image [18]. Coupling the AFAM technique with the so- called piezo-mode [16,18–21] can additionally provide information about domain polarization and the orientation of the grains within the crystal lattice [20].

2. AFAM EXPERIMENTAL TECHNIQUE

An AFM cantilever clamped on one side and free on the other can be described as a micro-beam with a characteristic set of free resonance frequencies. The most common modes excited are either flexural or torsional. Values of the free flexural or torsional oscillations can be measured with e.g. an instrument such as a Dimension 3000 Nanoscope (Digital Instruments, Santa Barbara, Ca USA) or a Solver P47H (NT-MDT, Zelenograd, Russia) which were employed for this study. When the cantilever approaches the sample surface and finally touches it, the forces interacting between the cantilever tip and the surface modify the boundary condition of the vibrating cantilever [4,5]. As a result, the resonance frequencies shift to higher values. These resonance frequencies are called contact resonance frequencies (Fig. 1 and Fig. 2). The values of free and contact resonance frequencies can be calculated as discussed previously [4,5]. From the difference of the contact resonance frequencies relative to the free resonances, one obtains the vertical or lateral contact stiffness [5, 22] which itself depend on both the elastic moduli of the sample and the tip, and their Poisson ratio, respectively [23,24]. As shown in Fig. 1, the tip contacts the sample surface over a certain contact area which is inferred indirectly by using a calibration material of known elasticity. Detailed information about tip-sample interactions and methods of evaluating local tip-sample contact stiffness can be found elsewhere [9,10,25]. Under certain circumstances, the local elastic modulus or the so-called indentation modulus M [24] can be derived from the contact stiffness [9,10,18]. At present the contribution of adhesion forces to the contact stiffness is made small in AFAM measurements by applying a sufficiently high static force on the cantilever so that the Hertzian contact forces are dominant [23]. When evaluating the vertical contact stiffness, the lateral forces to k^* are neglected. The indented volume is about $\pi r_h^2 \times 3r_h \approx 500\,\mathrm{nm}^3$ where r_h is the contact radius, here about 10 nm or less.

The contact resonance frequencies are excited by an ultrasonic transducer, which emits longitudinal waves or shear waves into the sample. Figure 2 displays the normalized contact resonance spectra of the first (Fig. 2a) and second (Fig. 2b) flexural mode measured on fused quartz, silicon, and sapphire. The spring constant

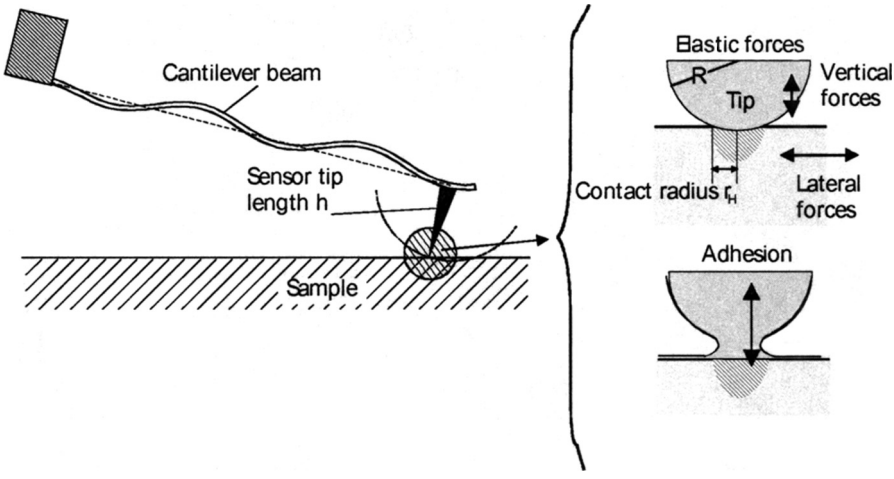

Figure 1. Principle of Atomic Force Acoustic Microscopy. Using the shift of the contact resonance frequencies relative to the free resonances, one can determine the local elastic constants of a material. The adhesion forces contribute to the measured vertical contact stiffness as well. Their influence can be neglected, provided the static forces are adjusted so that they are much larger than the adhesion forces.

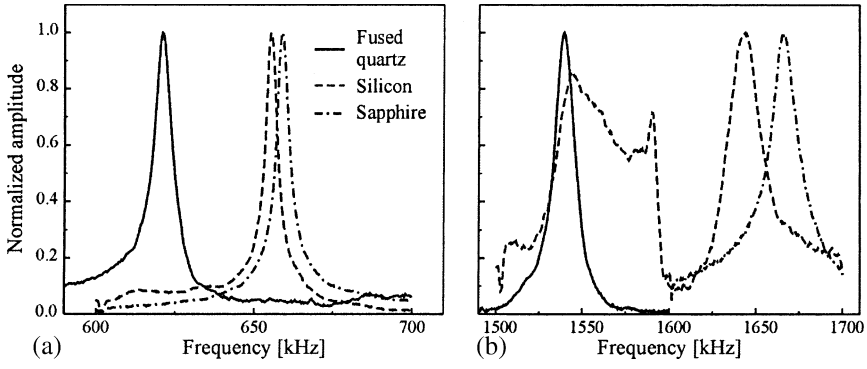

Figure 2. Normalized contact resonance spectra of the first (Fig. 2a) and second (Fig. 2b) flexural mode measured on samples with different elastic properties. The second mode on silicon shows a triple resonance.

of the cantilever was 44 N/m and the free resonance frequencies were 164 kHz and 1023 kHz for the first and second mode, respectively (not shown). The values of the indentation modulus of the reference samples varied from 77 (fused quartz), to 165 GPa (silicon), and to 423 GPa (sapphire). Very often double or triple resonance appear which are caused either by mode-coupling [26] or by multiple contacts between the tip and the surface.

In contact the resonance frequency varies during scanning and hence the amplitude and the phase of the cantilever vibration vary as well if the excitation frequency of the transducer is kept constant. This amplitude and phase contain information about the local tip-sample stiffness, and hence can be used as imaging quantities, see Fig. 3. It shows an AFAM-amplitude image of a lead calcium titanate film annealed at 650° C. The size of the images is $2 \times 2\,\mu m^2$. The cantilever material was coated with a conductive diamond-like layer. The overall spring constant was

44 N/m and the free resonance frequency of the first flexural mode of the cantilever was 188 kHz. The contrast seen in an amplitude image depends on the frequency of the applied ultrasound relative to the contact resonance frequency. At a frequency of 733 kHz the softer grains appear brighter than the stiffer grains (Fig. 3a). Imaging at a higher frequency, 791 kHz, the contrast of the image inverts (Fig. 3b) and the stiffer grains appear now brighter than the more compliant grains. This contract inversion has been known for a long time and has been noticed by several groups. Figure 4 shows an AFAM image of a nanocrystalline nickel sample based on monitoring the local contact resonance. From this measuring quantity, the local stiffness k^* is determined and then used as an imaging quantity. Values of the k^* ranged from 728 to 992 N/m. The tip used in this experiment was made from silicon, making it susceptible to tip wear [11]. The spring constant of the cantilever employed was 48 N/m and its free resonance frequencies were 166 and 1031 kHz for the first and second mode, respectively. The size of the image is $1.5 \times 1.4\,\mu m^2$. The image clearly shows ensemble of grains in the nanocrystalline structure.

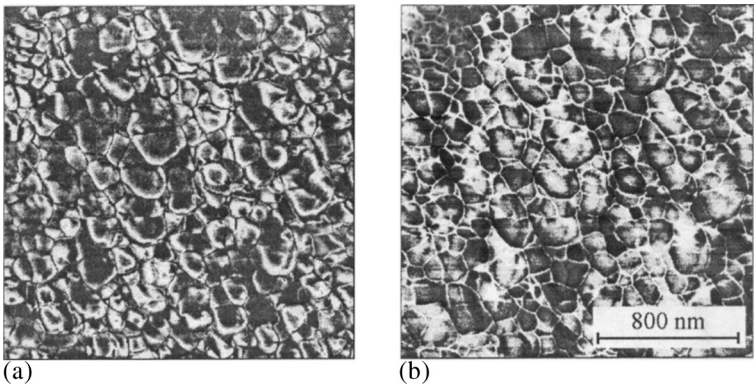

Figure 3. AFAM-amplitude images of a lead calcium titanate thin film annealed at 650° C. The contrast is caused by a shift of the resonance frequency when the contact stiffness changes locally. This in turn causes a change of the signal amplitude when the excitation frequency is kept constant.

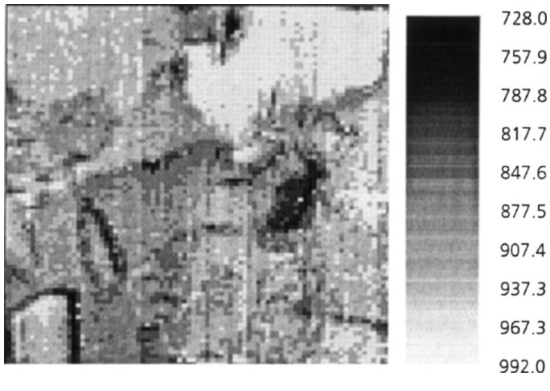

Figure 4. AFAM image of a nanocrystalline nickel sample. The contrast of the image is based on the contact stiffness comprising values between 728 N/m and 992 N/m. These values are determined from the contact resonances. The size of the image is $1.5 \times 1.4\,\mu m^2$.

In the so-called piezo-mode of atomic force microscopy an ac voltage is applied to a conductive AFM cantilever while scanning the surface of a piezoelectric material. The tip of the cantilever senses the local deformation of the surface caused by the electric field between the tip and a counter electrode (Fig. 5b, see also Fig. 10). Usually the ac frequency is far below the free resonance frequency of the AFM cantilever [16,17,19,20]. In $BaTiO_3$, an image series based on vertical and torsional cantilever vibration signals of the same surface area allowed the reconstruction of the domain orientation using this mode [20].

The piezo-mode technique can also be performed at frequencies in the range of the first free resonance of the cantilever [27]. In the images shown here, the ac frequency was set equal to a contact resonance frequency [28] which entails resonance amplification increasing the contrast and signal-to-noise ratio in an image. Figures 6a and 6b show images in the AFAM and ultrasonic piezo-mode for comparison. In contrast to AFAM amplitude images, piezo-mode images do not show contrast inversion when the excitation frequency is varied. Furthermore it can be seen that in the piezo-mode image (Fig. 5b) that there are areas with no piezo-activity (area with question mark). Comparing Fig. 5a with Fig. 5b, one can notice that areas of higher tip-sample contact stiffness correspond to areas where there is vertical piezo-activity. This can only happen if the polarization of the domains is dominantly vertical. The dark area in the AFAM image corresponding to low tip-sample contact stiffness can either be caused by an in-plane orientation of the domains or because the film is not piezoelectric at such locations and hence not ferroelectric. Further investigations will follow.

As mentioned above rectangular AFM cantilever beams can also be forced to torsional vibrations. In this case the experimental set-up is such that an ultrasonic transducer emits shear waves into the sample causing in-plane surface vibrations. The shear wave transducer is oriented so that the surface vibrations are polarized perpendicular to the long axis of the cantilever. If low excitation amplitudes (0.1 nm) are applied and if the excitation frequency is set close to a contact resonance frequency, the amplitude and the phase of the cantilever vibration contain now information about the local lateral tip-sample stiffness. Used as imaging quantity, they yield images of shear stiffness. By increasing the lateral excitation amplitude much above

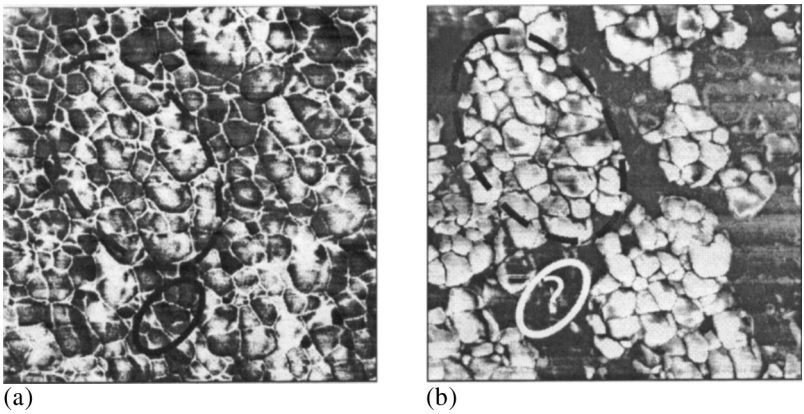

Figure 5. AFAM (a) and ultrasonic piezo-mode (b) images of the lead calcium titanate sample annealed at 650° C. The image in (a) is identical to the one in Fig. 3a.

0.1 nm, there is a change in the shape of the resonance curves. As shown recently [29] stick-slip between tip and sample occurs. This can be identified by taking local lateral spectra at one point of the sample: The maximum of the resonance curve increases linearly with the amplitude of the lateral displacement only at low excitation. At a certain threshold amplitude, the amplitude of the torsional vibrations does not increase any more and the resonance curve flattens out indicating the onset of sliding friction. Additionally, higher harmonics of the excitation signal appear which can be used for imaging. Such an image is shown in Fig. 6. A silicon sample was imaged first in the topography mode (Fig. 6a). At the excitation frequency of $f \approx 238\,\mathrm{kHz}$, an image was taken in the regime of stick-slip of the cantilever motion (Fig. 6b). Clearly an image could also be taken at 3f, here 714 kHz (Fig. 6c). It displays information related to the local friction coefficient. This new imaging mode is also at present the object of ongoing research.

3. APPLICATION OF AFM AND AFAM TO CRACK IMAGING

AFM and AFAM can be used to image cracks in ceramics in a similar way as can be done using SEM, Optical Microscopy or Scanning Acoustic Microscopy [30,31]. If one fractures a surface of a brittle material with a Vickers indenter, it is well-known and standard practice to infer from the length of the radial cracks the fracture toughness of the material [32]. There is much experience needed to determine reliably the length of the cracks with any of the microscopies. In this study the crack opening displacement U(x) was measured with an AFM. Measured close to the crack tip away from bridges in the wake of the crack, this would allow one to obtain information on K_{tip} using on the equation [33]

$$U(x) = \sqrt{8x/\pi}K_{tip}/E' \tag{1}$$

Figs. 7a and 7b show AFM images of Si_3N_4 ceramics where fracture was caused in bending specimens of the size $3 \times 4 \times 25\,\mathrm{mm}^3$ by a 10 kg load using a Vickers indenter. The size of the images is $30 \times 30\,\mu\mathrm{m}^2$. One can clearly see the cracks, however, it was difficult to exactly determine the origin of the cracks. Using the routine "section analysis" of the DI 300 AFM instrument, U(x) was measured as a function of x. When evaluating the data, a possible offset for the exact position of

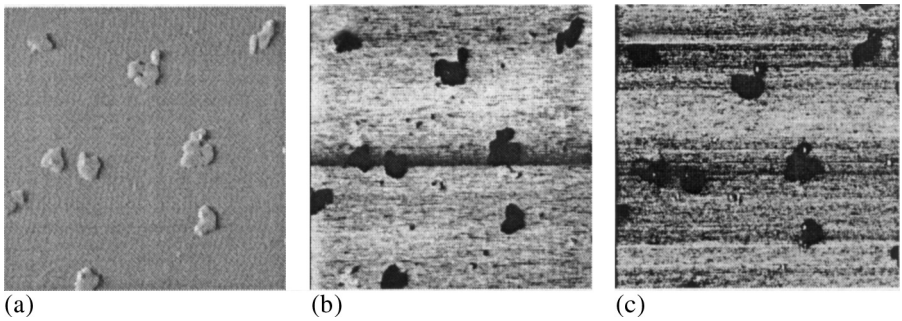

Figure 6. a) Topography of a Si-sample, b) Torsional amplitude $f = f_{excitation}$, c) Torsional amplitude $f = 3 \times f_{excitation}$.

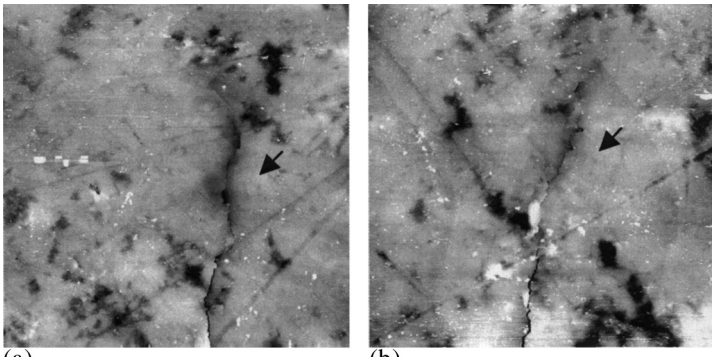

Figure 7. AFM topography images of two Si_3N_4 samples showing radial cracks caused by a Vickers indenter. The COD along the length of the radial cracks (arrows) was measured using standard routines of the DI instrument. A possible offset for the exact location of the tip was allowed in the analysis. The size of the image is 30H30 μm^2 and the topography scale was 120 nm (a) and 130 nm (b).

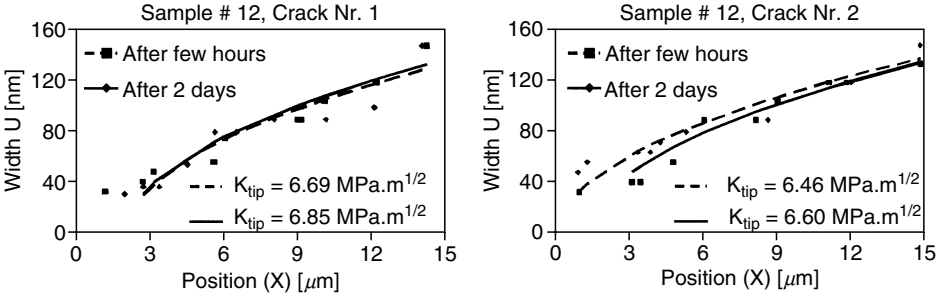

Figure 8. Crack opening displacement (COD) measured with an AFM in the topography mode. The figures display the width of the COD measured a few hours after the indent was made. The measurement was repeated after two days leading to a slight increase in the stress intensity factor. The data shown in Fig. 8a were obtained on the sample shown in Fig. 7a, and Fig. 8b corresponds to Fig. 7b.

the crack tip was taken into account. The reduced modulus E' for Si_3N_4 is 290 GPa. The value for K_{tip} was around 6.7 $MPam^{0.5}$ (Figs. 8) within the range of published data [32]. The high value indicates, however, that wake-effects played a role in the measurements, also the fact that the profile measured was not parabolic, see Figs. 8, as stipulated by Eq. (1)

We also studied in-situ crack propagation in an AFM by inducing cracks electrically, see Fig. 9. Poled PIC 151 PZT samples were loaded electrically with dc voltage of −900 V between the electrodes. Because the upper electrode was smaller than the ground electrode, an inhomogeneous electric field developed which was large enough to induce cracks due to the piezoelectric stresses.

Figure 10a shows a topography image of the environment of an individual crack in a crack field generated this way and Fig. 10b shows the corresponding AFAM image. Continued application of voltage led to additional cracking (Fig. 10c and 10d, arrow). Note that the AFAM images show also the domain structure opening the way to learn in-situ information on the role of the reorientation of domains in crack-shielding etc. which was much discussed during FCM8. Further studies are under way to clarify their role.

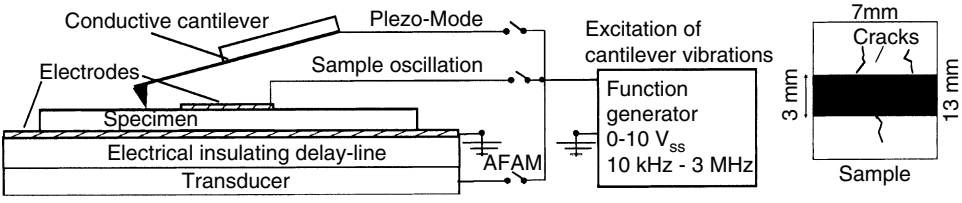

Figure 9. Configuration for the generation of in-situ cracks in an AFM allowing one to observe these cracks using the topography, the AFAM, and the ultrasonic piezo-mode. The insulating delay-line was necessary in order to protect the ultrasonic transducer from the applied dc voltages. The cracks emanate perpendicularly from the top electrode. The figure shows also the use of the electrodes for the ultrasonic piezo-mode.

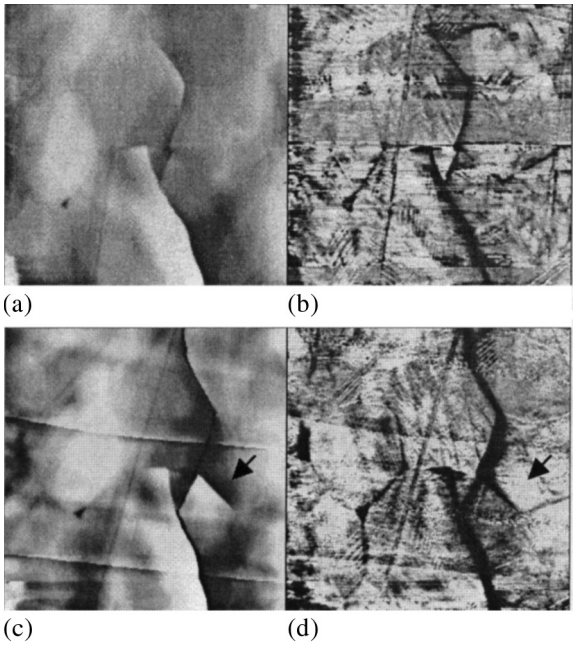

Figure 10. Observation of in-situ crack propagation after applying successive voltages up to −900 V to a PZT sample PIC 151; Fig. 10a: Topography image; Fig. 10b: AFAM image. The domain structure becomes visible. The images were taken with a cantilever having a spring constant of 47 N/m and at a static load of 1,8 μN. Continued voltage application leads to additional crack formation and reorientation of the domains (Fig. 10c and d, arrow). Image size of the individual images is 10H10 μm^2. The grey scale in the topography images comprises 70 nm.

Finally we studied crack propagation using the lateral stiffness as contrast in the images. Here the sensor tip vibrates in contact with the sample surface. An excitation frequency close to a torsional contact resonance frequency is selected. The torsional amplitude of the cantilever at this frequency is detected using the lateral channel of the AFM and a lock-in amplifier, and is then displayed as a color-coded image. A change in contact stiffness causes a shift of the contact resonance frequency and hence a change of cantilever vibration amplitude in the same manner as the vertical stiffness images, see above. Here also contrast inversion is observed. Cracks in a nanocrystalline ZrO_2 ceramic were generated by Vickers indents (Fig. 11). Fig. 11a

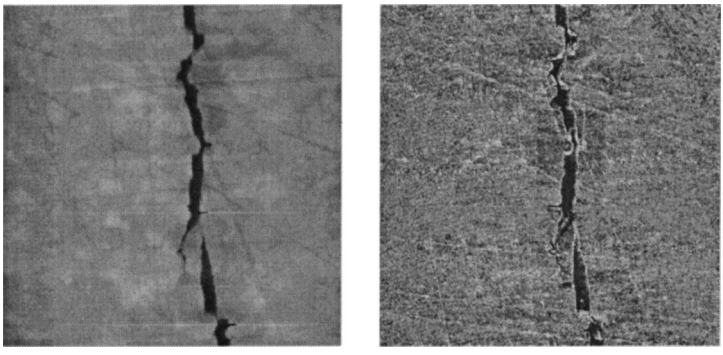

Figure 11. Topography (left) and lateral AFAM image (right) of a ZrO_2 ceramic.

shows topography, Fig. 11b the corresponding torsional resonance images of the identical surface areas. There are darker areas close to the crack flanks showing regions of altered elastic properties. This could be caused for example by the crack system below the surface and is examined further at present.

3. CONCLUSIONS

The AFAM and ultrasonic piezo-mode techniques described here lend itself for studying materials properties in ceramics on a nanoscale. Whereas the various imaging modes become more and more routine, the application of the AFM and ultrasonic AFM technique to study crack propagation are still in the early stage. However, the results presented here show that these techniques may provide much wanted information on the elastic, piezoelectric, and fracture mechanical behavior of ceramics during crack propagation.

4. ACKNOWLEDGEMENT

We gratefully acknowledge the financial support by the German Science Foundation. One of us (M.K-M) was supported by the SFB 277 at the University of the Saarland. Furthermore, it is a pleasure to thank D. Lupascu and J. Rödel for helpful discussions.

REFERENCES

1. P. Maivald, H.T. Butt, S.A. Gould, C.B. Prater, B. Drake, J.A. Gurley, V.B. Elings, and P.K. Hansma, Using Force Modulation to Image Surface Elasticities with the Atomic Force Microscope, *Nanotechnology* **2,** 103–106 (1991).
2. K. Yamanaka, H. Ogiso, and O. V. Kolosov, Ultrasonic force microscopy for nanometer resolution subsurface imaging, *Appl. Phys. Lett*. **64**, 178–180 (1994).
3. U. Rabe and W. Arnold, Acoustic Microscopy by Atomic Force Microscopy, in: *Proc. 21st Int. Symp. Acoustical Imaging*, edited by J. P. Jones, Plenum Press, New York, (1995) 585–592.

4. U. Rabe, K. Janser, and W. Arnold, Acoustic Microscopy with Resolution in the nm-Range, in: *Proc. 24th Int. Symp. Acoustical Imaging*, Eds. P. Tortoli, L. Masotti, Plenum Press, New York (1996) 669–676.
5. U. Rabe, K. Janser, and W. Arnold, Vibrations of Free and Surface-Coupled Atomic-Force Microscope Cantilevers: Theory and Experiment, *Rev. Sci. Instrum.* **67,** 3281–3293 (1996).
6. P. Vairac and B. Cretin, Scanning microdeformation microscopy in reflection mode, *Appl. Phys. Lett*. **68**, 461–463 (1996).
7. N.A. Burnham, G. Gremaud, A.J. Kulik, P.J. Gallo, and F. Oulevy, Scanning local-acceleration microscopy, *J. Vac. Sci. Tech*. **B14,** 794–799 (1996).
8. A. Rosa, E. Weilandt, S. Hild, and O. Marti, The simultaneous measurement of elastic, electrostatic and adhesive properties by scanning force microscopy: pulsed-force mode operation, *Meas. Sci. Technol*. **8,** 1333–1338 (1997).
9. E. Kester, U. Rabe, L. Presmanes, Ph. Tailhades, and W. Arnold, Measurement of Young's Modulus of Nanocrystalline Ferrites with Spinel Structures by Atomic Force Acoustic Microscopy *J. Phys. Chem. Solids* **61,** 1275–1284 (2000).
10. U. Rabe, S. Amelio, M. Kopycinska, S. Hirsekorn, M. Kempf, M. Göken, and W. Arnold, Imaging and Measurement of Local Mechanical Material Properties by Atomic Force Acoustic Microscopy, *Interf. and Surf. Analysis* **33,** 65–70 (2002).
11. S. Amelio, A. V. Goldade, U. Rabe, V. Scherer, B. Bhushan, and W. Arnold, Measurements of Elastic Properties of Ultra Thin Diamond-Like Carbon Coatings using Atomic Force Acoustic Microscopy, *Thin Solid Films* **392,** 75–84 (2001).
12. M. Prasad, M. Kopycinska, U. Rabe, and W. Arnold, Measurement of Young's Modulus of Clay Minerals Using Atomic Force Acoustic Microscopy, *Geophys. Res. Lett*. **29,** 13–16 (2002).
13. U. Rabe, S. Amelio, S. Hirsekorn, and W. Arnold, Imaging of Ferroelectric Domains by Atomic Force Acoustic Microscopy, in: *Proc. 25th Int. Symp. Acoustical Imaging*, edited by M. Halliwell and P.N.T. Wells, Kluwer Academic/Plenum Publishers, 253–260 (2000).
14. K. Yamanaka, Y. Maruyama, T. Tsuji, and K. Nakatomo, Resonance frequency and Q factor mapping by ultrasonic atomic force microscopy, *Appl. Phys. Lett*. **78,** 1939–1941 (2001).
15. A. L. Gruverman, J. Hatano, and H. Tokumoto, Scanning Force Microscopy Studies of Domain Structure in $BaTiO_3$ Single Crystals, *Jap. J. Appl. Phys*. **36,** 2207–2211 (1997).
16. P. Güthner and K. Dransfeld, Local poling of ferroelectric polymers by scanning force microscopy, *Appl. Phys. Lett*. **61**, 1137–1139 (1992).
17. A. Gruverman, O. Auciello, and H. Tokumoto, Scanning force microscopy: application to nanoscale studies of ferroelectric domains, *Integrated Ferroelectrics* **19,** 49–83 (1998).
18. U. Rabe, M. Kopycinska, S. Hirsekorn, J. Muñoz Saldaña, G.A. Schneider, and W. Arnold, High-resolution characterisation of piezoelectric ceramics by ultrasonic scanning force microscopy techniques, *J. Phys. D: Appl. Phys* **35,** 2621–2536 (2002).
19. K. Franke, J. Besold, W. Haessler, and C. Seegebarth, Modification and detection of domains on ferro-electric PZT films by scanning force microscopy, *Surf. Sci. Lett*. **302,** 283–288 (1994).
20. L. M. Eng, H.-J. Güntherodt, G. A. Schneider, U. Köpke, and J. Munoz Saldana, Nanoscale reconstruction of surface crystallography from three-dimensional polarization distribution in ferroelectric barium-titanate ceramics, *Appl. Phys. Lett*. **74,** 233–235 (1999).
21. S. Hong, J. Woo, H. Shin, J. U. Jeon, Y. E. Pak, E. L. Colla, N. Setter, E. Kim, K. No, Principle of ferroelectric domain imaging using atomic force microscope, *J. Appl. Phys*. **89,** 1377–1386 (2001).
22. V. Scherer, "*Ultraschall-Kraft-Mikroskopie mit lateraler Anregung*" Naturwisenschaftlich Technische Fakultät III. PhD-Thesis, University of the Saarland, (2002), unpublished.
23. K. L. Johnson, *Contact Mechanics* (Cambridge University Press, Cambridge, 1995).
24. G. M. Pharr, W. C. Oliver, F. Brotzen, On the generality of the relationship among contact stiffness, contact area, and elastic modulus during indentation, *J. Mat. Res*. **7,** 613–617 (1992).
25. K. Yamanaka, T. Tsuji, A. Noguchi, T. Koike, T. Mihara, Nanoscale elasticity measurement with in situ tip shape estimation in atomic force microscopy, *Rev. Sci. Instr*. **71,** 2403–2408 (2000).
26. M. Reinstaedtler, U. Rabe, V. Scherer, J.A. Turner, and W. Arnold, Imaging of flexural and torsional resonance modes of atomic force microscopy cantilevers using optical interferometry, *Surface Science*, (2003) in print
27. M. Labardi, V. Likodimos, and M. Allegrini, Force-microscopy contrast mechanisms in ferroelectric domain imaging, *Phys. Rev*. **B 61,** 14390–14398 (2000).

28. M. Kopycinska, U. Rabe, S. Hirsekorn, W. Arnold, Imaging of the Ferroelectric Domains Pattern in the Ultrasonic Piezo-Mode in: *Proc. 26th Acoustical Imaging, edited by R. Maev Kluwer Academic Publishers, New York, Acoustical Imaging*, **26,** 191–198 (2002).
29. M. Reinstädtler, U. Rabe, V. Scherer, U. Hartmann, A. Goldade, B. Bhushan, and W. Arnold, On the nanoscale measurement of friction using atomic-force microscope cantilever torsional resonances, *Appl. Phys. Lett*. **82,** 2604–2606 (2003).
30. W. Arnold, G. Weides, and S. Faßbender, Measurement of Elastic Properties Related to the R-Curve-Behavior of Ceramics, in: *Proc. of APCFS & ATEM '01 (Asian Pacific Conference on Fracture and Strength '01 and International Conference on Advanced Technology in Experimental Mechanics '01)*, The Japan Society of Mechanical Engineers, Tokyo, 2001, pp 517–522.
31. T.J. Marrow, G.A.D. Briggs, and S.G. Roberts, In-situ Acoustic Microscopy of Crack Bridging in Alumina, *J. Europ. Ceram. Soc*. **14,** 111–116 (1994).
32. B. Lawn, *Fracture of Brittle Solids*, in Cambridge Solid State Science Series (Cambridge University Press, 1995) pp. 249–306.
33. J. Rödel, J.F. Kelly, and B.R. Lawn, "In-situ Measurements of Bridging Crack Interfaces in the Scanning Electron Microscope", *J. Am. Soc*. **73,** 3313–3318 (1990).